ATIC EXPERIMENT: FLIGHT DATA PROCESSING

H. S. Ahn,[1] J. H. Adams,[2] G. Bashindzhagyan,[3] K. E. Batkov,[3] J. Chang,[4] M. Christl,[2] A. R. Fazely,[5] O. Ganel,[1] R. M. Gunasingha,[5] T. G. Guzik,[6] J. Isbert,[6] K. C. Kim,[1] E. Kouznetsov,[3] M. Panasyuk,[3] A. Panov,[3] W. K. H. Schmidt,[4] E. S. Seo,[1] R. Sina,[1] N. V. Sokolskaya,[3] J. Z. Wang,[1] J. P. Wefel,[6] J. Wu,[1] V. Zatsepin[3]
(1) University of Maryland, College Park, MD, USA
(2) Marshall Space Flight Center, Huntsville, AL, USA
(3) Skobeltsyn Institute of Nuclear Physics, Moscow State University, Moscow, Russia
(4) Max Plank Institute fur Aeronomie, Lindau, Germany
(5) Southern University, Baton Rouge, LA, USA
(6) Louisiana State University, Baton Rouge, LA, USA

Abstract

The Advanced Thin Ionization Calorimeter (ATIC) is a balloon borne experiment to measure the composition and energy spectra of Z = 1 to 28 cosmic rays over the energy range $\sim$ 30 GeV - 100 TeV. The instrument consists of a fully active 320-crystal Bismuth Germanate (BGO) calorimeter, 202 scintillator strips in 3 hodoscopes interleaved with a graphite target, and a 4480-pixel silicon matrix charge detector. ATIC has had two successful Long Duration Balloon flights from McMurdo, Antarctica: from 12/28/00 to 01/13/01 and from 12/29/02 to 01/18/03. We have developed the ATIC Data Processing Syetem (ADPS), which is an Object Oriented data processing program based on ROOT. In this paper, we describe the processing scheme used in handling the flight data, especially the calibration method and the event reconstruction algorithm.

1. Introduction

ATIC had two successful Long Duration Balloon flights from McMurdo, Antarctica in 2000 and 2002, collecting 45 GB and 65 GB of data, respectively. The details of the instrument is described in [4]. The flight data has been studied and processed using the ATIC Data Processing System (ADPS) based on ROOT [2], the capability of which has been described in other papers [1, 3]. In this paper, we focus on the detailed procedure of calibration and event reconstruction.

pp. 2109–2112

2. Calibration

2.1. Pedestal Correction: The Si pedestal was temperature dependent (30 ADC counts/°C), and thus exhibited a drift of 1 ADC count over 6 minutes. To account for this drift, pedestals taken every 6 minute were applied to science events collected during the following 6 minutes. The calorimeter and hodoscopes, however, showed little time dependence over the entire length of the flight, allowing pedestal correction based on hourly calibration runs.

The calorimeter and hodoscopes periodically suffered significant pedestal value jumps beyond the normal Gaussian distributions. Electronically, each chip had 16 channels which showed a coherent behavior of jumping by the same increment simultaneously. Each chip had several channels that were not connected to PMT outputs. These unconnected channels were used to estimate and correct the pedestal jump. The increment was estimated by taking the average of each unconnected channel's pedestal jump from the mean of its Gaussian distribution.

2.2. Low Range Calibration: The low-range responses for BGO crystals and scintillator strips were calibrated using cosmic-ray muons accumulated before the flight. After pedestal correction and off-line sparsification for each low-range channel, a tracking algorithm, described below, was applied. For channels that participated in the tracking, ADC distributions were plotted and fitted to locate the most probable value after angle/attenuation correction, as shown in Fig. 1. The responses for Si pixels were calibrated in a similar way using cosmic-ray Helium candidates accumulated during the flight. Comparing these most probable values among crystals/strips/pixels allowed the relative inter-crystal/strip/pixel calibration.

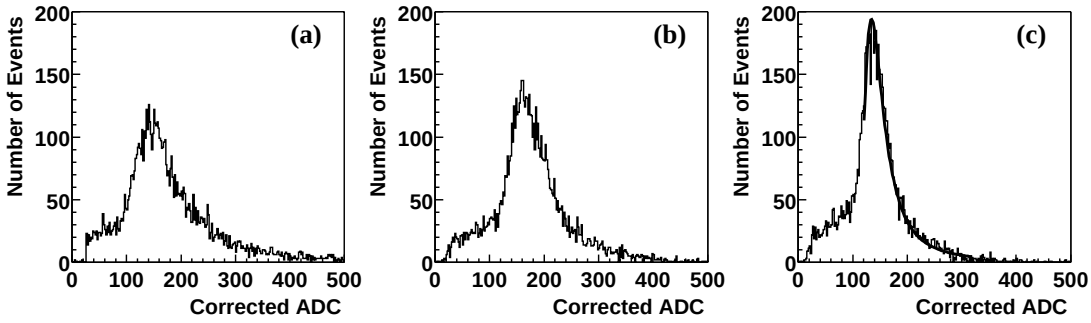

Fig. 1. ADC count distributions from cosmic ray muons passing through a scintillator strip after (a) pedestal correction, (b) attenuation correction, and (c) angle correction.

The electronics for the Si matrix and scintillator hodoscopes showed nonlinearity. In-flight charge-injection calibration runs taken every hour were used to correct this effect in the Si matrix. The hodoscopes showed saturation of the

readout electronics. Assuming the readout was linear when charge input was relatively small, the low range non-linearity was parametrized by comparing with high range signals, as shown in Fig. 2(a).

2.3. Higher Range Calibration: The higher-range responses were calibrated using cosmic ray showers accumulated during the flight. Two-dimensional distributions were made, as shown in Fig. 2, for two different ranges for crystals/strips. Linear fit to the distributions was used to estimate the range ratio, which was then used to calculate the higher-range calibration constants.

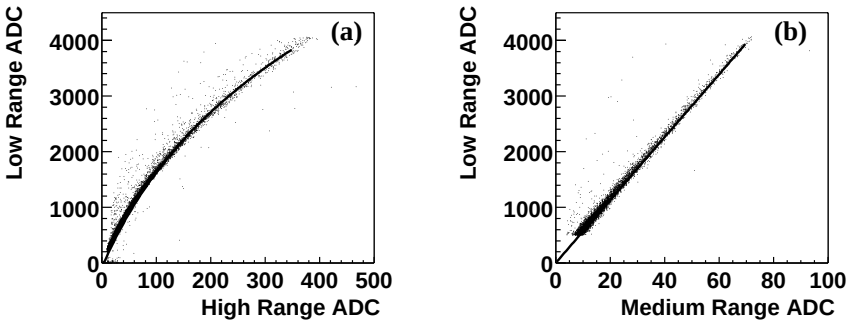

Fig. 2. Two-dimensional distributions for ADC counts of 2 different ranges from cosmic ray showers in (a) scintillator strip, and (b) BGO crystal.

2.4. Energy Conversion: The raw pulse height amplitude was converted to physical energy units following the steps described above. The calorimeter and hodoscopes had multi-range readouts using dynode pick-offs to cover the required dynamic range. For these, the lowest non-saturating range was selected and gain-corrected. The ADCs of the calorimeter and hodoscopes also suffered from an over-saturation problem. That is when the charge input was much higher than the saturation limit, the ADC output fell below the saturated values. To solve this problem, the higher range was selected and gain-corrected when its count was larger than the value at which the lower range was expected to saturate.

3. Event Reconstruction

3.1. Tracking: A new tracking algorithm was developed to efficiently select the particles that came within the detector geometry (e.g., passing all detector layers, from Si to the bottom BGO layer). The algorithm is based on the assumption that a high energy incident particle that came within the geometry is likely to deposit more energy in the layer segment along the incident axis than in the neighbor segments through all the layers. After a linear χ^2 fitting among all the possible combinations of the layer segments being done, the combination having low enough χ^2 and the maximum SNE (sum of normalized energy) defined below,

was selected as comprising the most probable track,

$$SNE(j_1, j_2, \cdots, j_N) \equiv \sum_{i=1}^{N} \frac{E_{j,i}}{E_{max,i}}, \quad (1)$$

where N, $E_{j,i}$ and $E_{max,i}$ represent the number of layers, the energy of the jth segment in the ith layer and the maximum energy in the ith layer, respectively. This algorithm was tested using GEANT/FLUKA 3.21 simulation with protons, and its position resolution is compared in Fig. 3(a) with those of conventional algorithms based on the center of mass concept.

3.2. Charge Determination: To determine the incident particle charge, the Si pixel that participated in the selected track was compared with those of its neighbors. When one of the neighbors had consistent charge, the average was taken as the reconstructed charge. Otherwise, the maximum charge among the pixels was taken. The charge distribution for hydrogen and helium is shown in Fig. 3(b).

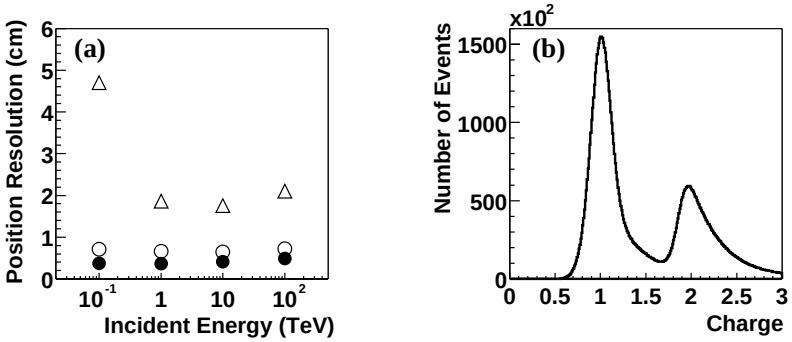

Fig. 3. Results of event reconstruction, (a) position resolution of the new tracking algorithm (filled circle) from proton simulations, compared with only BGO (triangle) and BGO/Scintillator/Si (open circle), and (b) charge distribution for hydrogen and helium from the ATIC 2000 flight.

Acknowledgment

This work was supported by NASA grant NAG5-5308 at UMD, by NASA grants at LSU, SU and MSFC and by the Russian Foundation of Basic Research at MSU.

References

1. Ahn, H. S., et al., Proc. 27th ICRC (Hamburg), Vol. 6, 2119 (2001)
2. Brun, R., Rademakers, F., Nucl. Instr. Meth. A389, 81 (1997)
3. Ganel, O., et al., Proc. 26th ICRC (Salt Lake City), Vol. 5, 453 (1999)
4. Guzik T. G., et al., Proc. 26th ICRC (Salt Lake City), Vol. 5, 9 (1999)